Published in final edited form as:
Nature. 2008 September 25; 455(7212): 537–541. doi:10.1038/nature07265.

Functional auditory hair cells produced in the mammalian cochlea by *in utero* gene transfer

Samuel. P. Gubbels[1,*,†], **David W. Woessner**[1,*], **John C. Mitchell**[2], **Anthony J. Ricci**[3], and **John V. Brigande**[1]

[1]Department of Otolaryngology, Oregon Hearing Research Center, Oregon Health & Science University/NRC04, 3181 SW Sam Jackson Park Road, Portland, OR 97239, USA

[2]Department of Biomaterials and Biomechanics, School of Dentistry, Oregon Health & Science University, 3181 SW Sam Jackson Park Road, Portland, OR 97239, USA

[3]Department of Otolaryngology-Head and Neck Surgery, Stanford University School of Medicine, 801 Welch Road, Stanford, CA 94305, USA

Abstract

Sensory hair cells in the mammalian cochlea convert mechanical stimuli into electrical impulses that subserve audition[1,2]. Loss of hair cells and their innervating neurons is the most frequent cause of hearing impairment[3]. Atonal homolog 1 (*Atoh1*, also known as *Math1*) is a basic helix-loop-helix transcription factor required for hair cell development[4-6] and its misexpression *in vitro*[7,8] and *in vivo*[9,10] generates hair-cell-like cells. *Atoh1*-based gene therapy to ameliorate auditory[10] and vestibular[11] dysfunction has been proposed. However, the biophysical properties of putative hair cells induced by *Atoh1* misexpression have not been characterized. Here we show that *in utero* gene transfer of *Atoh1* produces functional supernumerary hair cells in the mouse cochlea. The induced hair cells display stereociliary bundles, attract neuronal processes, and express the ribbon synapse marker C-terminal binding protein 2 (*Ctbp2*)[12,13]. Moreover, the hair cells are capable of mechanoelectrical transduction[1,2] and display basolateral conductances with age-appropriate specializations. Our results demonstrate that manipulation of cell fate by transcription factor misexpression produces functional sensory cells in the postnatal mammalian cochlea. We anticipate that our *in utero* gene transfer paradigm will enable the design and validation of gene therapies to ameliorate hearing loss in mouse models of human deafness[14,15].

We devised an *in utero* gene transfer paradigm to conduct gain-of-function studies in the developing mouse inner ear[16] (Fig. 1 and Supplementary Figs. 1 and 2). A plasmid consisting of the human elongation factor 1-α (EF1α) promoter[17] driving expression of a destabilized form (2hr half-life) of green fluorescent protein (ZsGreen)[18, 19] was microinjected through the uterus into the fluid-filled cavity of the embryonic day 11.5 (E11.5) mouse otic vesicle (Fig. 1a and Supplementary Video 1). The plasmid-filled left

Correspondence and requests for materials should be addressed to J.B. (brigande@ohsu.edu).
*These authors contributed equally to this work.
†Present Address: Department of Surgery, Division of Otolaryngology, University of Wisconsin – Madison, K4/719 CSC, 600 Highland Avenue, Madison, WI 53792, USA

Supplementary Information is linked to the online version of the paper at www.nature.com/nature.

Author Contributions The project was conceived by J.B. Experiments were planned and performed by S.G. and D.W. with advice from J.B. and analyzed by S.G., D.W. and J.B. J.B. performed the experimental embryology. A.R. conducted the electrophysiology experiments and interpreted the results. J.M. acquired the scanning electron micrographs. J.B. and A.R. co-wrote the paper.

Author Information The authors declare no competing interests.

otocyst was centered in the field of a paddle-style, circular electrode and a directional, square wave pulse train was delivered to electroporate ventral progenitor cells that give rise to the organ of Corti (Fig. 1b and Supplementary Video 2). ZsGreen was detected 24hrs post-electroporation in a tear drop-shaped pattern consistent with the morphology of the otocyst (4/6 otocysts; Fig. 1c and Supplementary Fig. 2). Histological analysis revealed ZsGreen$^+$ progenitor cells in their stereotyped pseudostratified arrangement within the otic epithelium (Fig. 1d)[20]. These data indicate that *in vivo* electroporation transfects otic epithelial progenitor cells in the ventromedial otocyst and produces robust transgene expression within 24hrs.

To determine which differentiated cell types arise from transfected otic progenitors, we injected and electroporated EF1α-enhanced GFP at E11.5 and analyzed E18.5 cochlear whole mounts immunostained for the hair cell marker, myosin 7a (Myo7a)[21, 22]. The gross morphology of the E18.5 inner ear was unaffected and electroporated embryos carried to term have normal auditory function one month after birth (Supplementary Table 1). Robust GFP expression was present in inner and outer hair cells and supporting cells in the E18.5 organ of Corti (Fig. 2a,b,d,f and Supplementary Fig. 3). Remarkably, the distribution of transfected cells in the cochlea was constrained to the organ of Corti proper. Differential regulation of GFP expression by the EF1α promoter may account for this restricted pattern. These data indicate that *in vivo* electroporation transfects otic progenitors that give rise to all of the constituent cell types within the organ of Corti but it does not adversely affect gross embryonic development or the postnatal acquisition of hearing.

To induce otic epithelial progenitor cells to adopt a hair cell fate, we misexpressed *Atoh1*, a basic helix-loop-helix transcription factor required for hair cell formation[4]. A plasmid generating a bicistronic message encoding Atoh1 and enhanced GFP was injected and electroporated in the E11.5 otocyst. The gross distribution of Atoh1/GFP expression in the E18.5 cochlea appeared to follow that defined by Myo7a (Fig. 1e), suggesting that progenitors giving rise to the organ of Corti were transfected with *Atoh1*. Atoh1/GFP$^+$ cells co-expressing Myo7a were present in the base, midbase, and apex of transfected cochleae (Fig. 2c,e,g). The stereotyped pattern of one inner and 3 outer rows of hair cells was altered by the overabundance of Atoh1/GFP$^+$/Myo7a$^+$ cells that we refer to as supernumerary cells (Fig. 2c,e,g). The apical surfaces of the supernumerary cells displayed phalloidin$^+$ epithelial protrusions at E18.5 that resemble immature stereociliary bundles (Supplementary Figure 4a-d) which persist one month after birth (Fig. 2h-k). Ectopic Myo7a$^+$ cells displaced from the organ of Corti toward the modiolus were occasionally observed (Fig. 2c,e and Supplementary Figure 4f).

The total number of Myo7a$^+$ cells (i.e., putative hair cells, whether transfected or not) in the cochlear base was increased 1.8 fold and 50% of these cells were Atoh1/GFP$^+$ (Supplementary Table 2). In addition, we detected a 2.2-fold increase in putative inner hair cells (IHCs) and a 1.5-fold increase in putative outer hair cells (OHCs) in the base. Consequently, the OHC:IHC ratio shifted from 3.4:1 to 2.4:1 owing to the disproportionate increase in IHCs. Little is known about inner and outer hair cell fate specification and if the cues responsible are temporally or spatially regulated (or both). *In utero* gene transfer of *Atoh1* at different stages of otic vesicle development may provide insights into the molecular mechanisms governing hair cell fate specification.

There were fewer supernumerary Myo7a$^+$ cells generated in the midbase (1.2 fold increase; 40% Atoh1/GFP$^+$), and none in the apex (Supplementary Table 2). The observed base-to-apex gradation in the abundance of supernumerary Myo7a$^+$ cells is inversely associated with the gradient of cell cycle exit in the organ of Corti in which apical progenitors exit the cell cycle first and basal progenitors exit last[5, 23]. We hypothesize that the large increase in

supernumerary hair cells in the base results from clonal expansion of *Atoh1*-transfected progenitors.

To test if the supernumerary Atoh1/GFP$^+$/Myo7a$^+$ cells attracted nerve fibers, we labeled neurons in the cochlear nucleus in retrograde fashion[24] and analyzed the distribution of labeled processes to the organ of Corti. A cluster of 4 Atoh1/GFP$^+$/Myo7a$^+$ cells in the OHC region attracted a cluster of NeuroVue Red-labeled fibers[25] (Fig. 3a, arrowhead) whose density was enriched at the base of the cluster (Fig. 3a, inset, arrowhead). An isolated Atoh1/GFP$^+$ cell in the same organ of Corti (Fig. 3a, arrow) attracted a refined NeuroVue$^+$ fiber to its base (Fig. 3a, inset, arrow). To corroborate that the labeled fibers are neuronal processes, we analyzed neurofilament distribution in Atoh1/GFP-transfected cochleae. We detected neurofilament$^+$ processes terminating at the base of both untransfected Myo7a$^+$ cells and Atoh1/GFP$^+$/Myo7a$^+$ cells (Fig. 3b and Supplementary Video 3). We next sought to determine if the Atoh1/GFP-transfected cells expressed C-terminal binding protein 2 (Ctbp2), a marker of the hair cell ribbon synapse, at postnatal day 35 (P35). We detected discrete foci of Ctbp2 in the basolateral domain in 20 of 39 Atoh1/GFP$^+$ cells from 2 cochleae (Fig. 3c,d and Supplementary Video 4). These data suggest that Atoh1/GFP$^+$ cells engage a synaptogenic program and are innervated by neurons that associate with the cochlear nucleus.

Hair cells convert mechanical stimuli into electrical impulses and display a distinct set of biophysical properties. To further characterize the identity of Atoh1/GFP$^+$ cells, we interrogated their electrophysiological properties at P4-6. Cells were selected and grouped based on whether they were GFP$^+$ or GFP$^-$ and whether they had the morphological phenotype of an IHC or an OHC. Morphology was based on the shape of the hair bundle viewed with differential interference contrast microscopy, with OHCs having the classical V-shape and the IHCs being straight. OHCs were located on the strial side of pillar cells and IHCs were located on the modiolar side (Fig. 2a). Supernumerary IHCs and OHCs were investigated. The ectopic cells displaced toward the modiolus were structurally unstable and could not be patch clamped (Supplementary Figure 4f). Comparisons were made both between cell types and within types for GFP$^+$ and GFP$^-$ cells. Where no differences were observed, data were pooled.

No difference was observed in zero-current potential between GFP$^+$ and GFP$^-$ hair cells, or between IHCs and OHCs, with values of -63 ± 13mV (n = 5) compared to -49 ± 15mV (n = 7), respectively. Although membrane capacitance was not different between GFP$^+$ and GFP$^-$ cells, capacitance was different ($p < 0.001$, two-tailed t-test) between IHCs and OHCs with values of 7.3 ± 1.3pF (n = 11) and 4.7 ± 1.5pF (n = 24), respectively. These results indicate that Atoh1/GFP-transfected and untransfected cells elaborated differential capacitances consistent with their identities as inner or outer hair cells.

Mechanotransduction was investigated by stimulating hair bundles with a piezo-driven glass fiber (Fig. 4a)[26]. We found that hair cells induced by *Atoh1* misexpression displayed the same range of current amplitudes, sensitivity, and adaptation as non-GFP expressing hair cells. Figure 4 shows this analysis for GFP$^+$ and GFP$^-$ OHCs. Current amplitudes varied considerably as expected, in part due to the developmental age at which they were measured[26]. Peak currents of 152 ± 107pA (n = 15) and 200 ± 177pA (n = 7) were measured for GFP$^+$ and GFP$^-$ cells, respectively (Fig. 4b, c). Normalized current-displacement plots (Fig. 4d) were fit with a single Boltzmann function and no differences were found in either half activating displacement or sensitivity with values of 0.54 ± 0.06μm and 0.53 ± 0.02μm and slopes of 0.17 ± 0.05μm^{-1} and 0.17 ± 0.03μm^{-1} ($r^2 = 0.99$ for both) for GFP$^+$ and GFP$^-$ cells, respectively. Adaptation kinetics were compared by fitting the response to a positive stimulus that elicited less than 50% of the maximal response with the equation for a double

exponential[27]. Fast and slow time constants did not differ between groups and gave values of 0.81 ± 0.48ms (n = 6) and 0.39 ± 0.3ms (n = 4) for the fast and 8 ± 10ms and 8 ± 6ms for the slow time constants for GFP^+ and GFP^- OHCs. These results suggest that mechanotransduction follows a normal developmental progression in Atoh1/GFP^+ hair cells[26].

Basolateral conductances were also investigated (Fig. 4e-m). A voltage protocol (Fig. 4e) that first prepulsed the potential from -84mV to -120mV for 200ms was used to determine if inactivating conductances were present. Both inward and outward currents were observed (Fig. 4f,g,i). The outward currents did not vary in current amplitude or activation properties between GFP^+ and GFP^- cells; however, there was a difference ($p < 0.001$) between OHCs and IHCs in current amplitude with OHCs having a peak current of 1878 ± 653pA (n = 29) and IHCs having a peak current of 2790 ± 767pA (n = 14). These results again demonstrate that Atoh1/GFP^+ cells develop outward current characteristics consistent with their terminal differentiation as inner or outer hair cells.

Rapidly activating, rapidly inactivating inward currents were observed in 90% of the GFP^+ OHCs, but only 30% of GFP^- cells (Fig. 4f,g,i-m). The trend was less apparent for IHCs with 80% of GFP^+ and 66% of GFP^- IHCs having inward currents. The greatest difference in the inward current is depicted in Fig. 4i; the GFP^+ OHCs had much larger current amplitudes than did the GFP^- cells with peak currents of 1998 ± 1178pA (n = 19) and 475 ± 100pA (n = 3), respectively ($p< 0.05$). Persistent, strong expression of Atoh1/GFP at postnatal stages by the EF1α promoter may underlie the difference in current amplitude observed. No difference was found in activation properties between any of the groups. Inactivation was not different between GFP^+ and GFP^- cells but again there was a difference in the half inactivation between GFP^+ IHCs and OHCs with values of -78 ± 1mV and -71 ± 1mV, respectively ($p<0.01$, n = 4 for each). No difference was found for the slope with values of 6.0 ± 1mV^{-1} and 5.5 ± 0.4mV^{-1} for IHC and OHC, respectively. These data support the conclusion that misexpression of *Atoh1* leads to the production of functional sensory hair cells in the postnatal cochlea that elaborate electrophysiological specializations consistent with inner or outer hair cell identity.

There is intense interest in gene[10, 11] and cell[28, 29] replacement strategies to restore auditory and vestibular function in the diseased inner ear. While *Atoh1* misexpression in cochlear cultures[7, 8] and in the adult guinea pig inner ear[9, 10] generates cells with some of the morphological and molecular characteristics of sensory hair cells, electrophysiological analysis of the induced hair cells was not conducted. We microinjected expression plasmid encoding Atoh1 into the nascent mouse otocyst and subsequently transfected otic epithelial progenitor cells by *in vivo* electroporation. The induced supernumerary hair cells express Myo7a, attract neurofilament-bearing processes, and localize the ribbon synapse marker Ctbp2 to their basolateral domain. In addition, the induced hair cells mechanotransduce and possess basolateral currents consistent with their maturational stage. Our work establishes that supernumerary cells induced by electroporation-mediated gene transfer of *Atoh1* are functional sensory hair cells. The ability to conduct gain-of-function experiments in the developing mammalian inner ear by *in utero* gene transfer may enable the design and functional assessment of gene therapies aimed at ameliorating hearing loss and vestibular dysfunction in mice that model human deafness and balance disorders. This capability is a crucial first step in defining translational therapies to ameliorate the devastating effects of inner ear disease in humans.

Methods Summary

Experimental embryology. Timed pregnant dams were laparotomized to externalize the uterus. Four to 6 otocysts were injected and electroporated per dam. Transfected inner ears were harvested at E12.5, E18.5, P4-6, or P28-35 and fixed in 4% paraformaldehyde in phosphate buffered saline (PBS) prior to cryosectioning, nerve tract tracing, scanning electron microscopy, or immunohistochemistry. **Nerve tract tracing**. The E18.5 crania were sagitally hemisected and nylon filter coated with NeuroVue Red was inserted into the cochlear nucleus followed by 7 day incubation at 37°C in PBS/0.1% sodium azide. Nerve tracts were visualized by confocal microscopy in cochlear whole mounts immunostained for Myo7a. **Scanning electron microscopy**. The OTOTO method was performed[30]. **Video**. Confocal stacks of immunostained cochleae were processed with Imaris software to generate 3-D images and video. **Cell quantification**. The base, midbase, and apex of transfected E18.5 cochleae immunostained for Myo7a were imaged by confocal microscopy. The mean number of hair cells, transfected hair cells, and transfected supporting cells was counted per 100μm field ± standard error of the mean and the Mann-Whitney U Test was used for statistical comparisons. **Electrophysiology**. Hair cells were patch clamped with an axoclamp 200b amplifier coupled to a 1322 digidata A/D, D/A board driven by JClamp software. Soda glass pipettes, resistances 1-3 MΩ, coated with ski wax were used to record from both GFP^+ and GFP^- cells. Mechanical stimulation was accomplished with a stiff glass probe attached to a piezoelectric stack. Stimuli were filtered at 20kHz and differentially amplified through an attenuator to regulate stimulus amplitudes. Data was sampled at 40 kHz, filtered at 10 and each stimuli is an average of 8 samples. Junction potential and series resistance were corrected offline. No leak subtraction was applied. Data are presented as mean ± standard deviation and two-tailed t-tests were used for statistical comparisons.

Methods

Expression plasmid construction

EF1α-GFP: pBMN-IRES-GFP (gift from G. Nolan) and pEF1α-GFP (gift from C. Cepko) were cut with EcoRI/BsrGI to excise IRES-GFP and GFP, respectively. IRES-GFP was then ligated to the pEF1α vector to form pEF1α-IRES-GFP. EF1α-ZsGreen: The EF1α promoter from pEF1α-GFP was subcloned into pGEM using SalI. A plasmid with EF1α in the correct orientation was then digested with SalI/EcoRI and the promoter fragment was ligated into pZsGreen1-DR (Clontech, Mountain View, CA) linearized with XhoI/EcoRI. pEF1α-Atoh1-IRES-GFP: Gateway-enabled destination vector pEF1α-RfC.1-IRES-GFP was created using the Gateway Vector Conversion System (Invitrogen, Carlsbad, CA) by digesting pEF1α-IRES-GFP with EcoRI, blunting the ends, and inserting Reading Frame Cassette C (RfC.1). Atoh1 cDNA was obtained from ATCC (MGC-19141) and the open reading frame (ORF) was amplified with the following primers: (5′-GGGGACAAGTTTGTACAAAAAAGCAGGCTTAATGTCCCGCCTGCTGCAT-3′ and 5′-GGGGACCACTTTGTACAAGAAAGCTGGGTACTAACTGGCCTCATC-AGA-3′). A BP reaction was performed with Atoh1 cDNA and the donor vector pDONR/Zeo creating pENTR-Atoh1/Zeo. The subsequent LR reaction between pENTR-Atoh1/Zeo and pEF1α-RfC.1-IRES-GFP generated the expression plasmid pEF1α-Atoh1-IRES-GFP.

Expression plasmid purification

Expression plasmids were prepared with the Qiagen HiSpeed Plasmid Maxi Kit with modification. The plasmid was 0.22μm filtered prior to ethanol precipitation, resuspended in sterile PBS at 3μg/μL, and stored at -20°C. Crystalline fast green was added to a freshly thawed aliquot to aid visualization during microinjection.

Timed pregnant breeding

Noon on the day a vaginal plug was detected was designated embryonic day 0.5 (E0.5) of development. Our initial experiments to define efficacious electroporation parameters were conducted with CD1 mice owing to their fecundity. CD1 mice, however, display elevated auditory thresholds by the 4th postnatal week. We outcrossed CD1 females with C57BL/6NTac males to generate CD1/B6 mice that have normal auditory brainstem responses through P35. Electrophysiology was conducted on hair cells in the CD1/B6 postnatal organ of Corti.

Experimental embryology

Dams were anesthetized with 7.2 μL/g body weight of a solution containing 9mg/ml Nembutal, 20.8 mg/ml magnesium sulfate heptahydrate, 40% propylene glycol, and 10% ethanol. The bicornate uterus was externalized by ventral laparotomy. A soft-cable fiber optic light guide was pressed lightly against the irrigated uterus to illuminate the rostral and caudal branches of the primary head vein between which the otic vesicle resides (See Supplementary Video 1). Microinjection pipettes were fabricated with an 18-24μm outer diameter and 20 degree bevel. The pipette was advanced through the uterus, extraembryonic membranes, and into the fluid-filled lumen of the otocyst. Expression plasmid tinted with fast green tracking dye was pressure injected (~7-9, 10msec pulses per otocyst at 10-15psi) into the lumen of the vesicle with a Picospritzer III (source gas nitrogen, 99.9% purity). The plasmid-filled otocyst was centered in the circular, 5mm field of the tweezer-style electrode paddles by securing the uterus with a gentle grip from the cathode and anode disks. A train of 5 square wave pulses (43volts/pulse at 50msec/pulse and 950msec interpulse delay) was delivered to drive the plasmid into ventral otic epithelial progenitors.

Immunohistochemistry

Embryos were harvested 24hr or 6-7 days post-electroporation and fixed in 4% paraformaldehyde-PBS (PFA/PBS; pH 7.2-7.4) for 8-12hr at 4°C with gentle agitation. Postnatal mice were fixed by cardiac perfusion with PFA/PBS and inner ears were decalcified in disodium EDTA. For cryostat sections, the entire E12.5 head was cryoprotected in graded sucrose/PBS to 30%, embedded in OCT medium, and serially sectioned at 12 μm in the coronal plane. For whole mounts, the cochlea was dissected free of the cartilaginous capsule and the lateral wall was removed. The cryostat sections or dissected cochleae were permeabilized and blocked in 0.2% saponin in blocking solution (PBS containing 1% bovine serum albumin and 3% serum from the species in which the secondary antibody was generated). Myo7a and neurofilament antibodies were applied overnight at 4°C with gentle agitation. Alexa Fluor conjugated secondary antibody was applied for 2hr at room temperature. Phalloidin-Alexa Fluor conjugates were applied for 30min at room temperature in PBS. Sectioned cochleae and the base, midbase, or apex of whole mount cochleae were covered in VectaShield (Vector Laboratories, Burlingame, CA) prior to epifluorescence or confocal analysis. Antibodies and labeling reagents used were: Alexa 660-conjugated phalloidin (dilution 1/50; A22285, Molecular Probes, Eugene, OR); Myosin 7a (dilution 1/150; 25-6790, Proteus Biosciences Inc, Ramona, CA;); neurofilament (dilution 1/1000; ab10586, Abcam Inc., Cambridge, MA); Alexa 568-conjugated goat anti-rabbit (dilution 1/300; A11036, Molecular Probes); and Cy5-conjugated goat anti-chicken (dilution 1/100; ab6569, Abcam Inc).

Electrophysiology

Electrophysiological investigations were performed on isolated organs of Corti between P4-P6. Tissue was isolated as described previously[25]. Isolated tissue was placed into a coverslip-bottomed recording chamber and held in place with single strands of dental floss.

The bath was perfused at a rate of 2.5 ml/min with a solution containing (in mM): 135 NaCl, 1 KCl, 10 4-(2-Hydroxyethyl)1-Piperazineethanesulfonic Acid (HEPES), 1.5 $CaCl_2$, 2 $MgCl_2$, 6 glucose, 4 pyruvate, 2 ascorbate, 2 creatine, pH was set at 7.4 and osmolality maintained at 325 mosml. The chamber and tissue were viewed with an Olympus BX51 microscope using a 60× water immersion lens and Nomarski optics (Olympus America, Center Valley PA); images were captured with a Hamamatsu C2400 (Bridgewater, NJ). Hair cells were patch clamped with an axoclamp 200b amplifier (Molecular Devices, Sunnyvale CA) coupled to a 1322 digidata A/D, D/A board (Molecular Devices) driven by JClamp software (SciSoft, New Haven CT). Soda glass (Garner Glass, Claremont, CA) pipettes, resistances 1-3 MΩ, coated with ski wax were used to record from both GFP^+ and GFP^- cells. The internal solution contained (in mM): 125 KCl, 10 HEPES, 5 MgATP, 5 Creatine Phosphate, 1 Ethylene glycol-bis(2-aminoethylether)-N,N,N′,N′-tetraacetic acid (EGTA), 2 ascorbate, the pH was balanced to 7.2 and the osmolality was kept at 295 mosml. Mechanical stimulation was accomplished with a stiff glass probe attached to a piezoelectric stack (Physik Instrumente, Irvine CA). Stimuli were filtered at 20kHz (Frequency Devices, Ottawa, IL) and differentially amplified through an attenuator to regulate stimulus amplitudes (PA5, Tucker Davis, Alachua, FL). Data was sampled at 40 kHz, filtered at 10 and each stimuli are an average of 8 samples. Junction potential and series resistance were corrected offline.

Supplementary Material

Refer to Web version on PubMed Central for supplementary material.

Acknowledgments

We thank C. Bresee and J. Jungwirth for expert technical support; C. Cepko and G. Nolan for plasmids EF1α-GFP and BMN-IRES-GFP, respectively; A. Kiernan, D. Fekete, S. Heller, A. Nguyen-Huynh, C. Bresee, and J. Jungwirth for critical comments that improved the manuscript; D. Trune, B. Fritzsch, and N. Segil for helpful discussions; S. Griest for statistical analyses; and M. Campbell and S. Nigra for exceptional animal care. This study was supported by grants from the National Institute on Deafness and Other Communication Disorders (J.B. and A.R.); the McKnight Endowment Fund for Neuroscience (J.B.); and the American Otological Society (Research Training Fellowship to S.G.).

References

1. Vollrath M, Kwan K, Corey D. The micromachinery of Mechanotransduction in Hair Cells. Annu Rev Neurosci 2007;30:339–365. [PubMed: 17428178]
2. Grant L, Fuchs PA. Auditory transduction in the mouse. Pflugers Arch 2007;454:793–804. [PubMed: 17534654]
3. Davis, A. Hearing disorders in the population: first phase findings of the MRC National Study of Hearing, in Hearing Science and Hearing Disorders. Lutman, M.; Haggard, M., editors. Academic Press; New York: 1993.
4. Bermingham NA, et al. Math1: an essential gene for the generation of inner ear hair cells. Science 1999;284:1837–1841. [PubMed: 10364557]
5. Chen P, Johnson JE, Zoghbi HY, Segil N. The role of Math1 in inner ear development: Uncoupling the establishment of the sensory primordium from hair cell fate determination. Development 2002;129:2495–2505. [PubMed: 11973280]
6. Jones JM, et al. Inhibitors of differentiation and DNA binding (Ids) regulate Math1 and hair cell formation during the development of the organ of Corti. J Neurosci 2006;26:550–558. [PubMed: 16407553]
7. Zheng JL, Gao WQ. Overexpression of Math1 induces robust production of extra hair cells in postnatal rat inner ears. Nat Neurosci 2000;3:580–586. [PubMed: 10816314]
8. Woods C, Montcouquiol M, Kelley MW. Math1 regulates development of the sensory epithelium in the mammalian cochlea. Nat Neurosci 2004;7:1310–1318. [PubMed: 15543141]

9. Kawamoto K, et al. Math1 gene transfer generates new cochlear hair cells in mature guinea pigs in vivo. J Neurosci 2003;23:4395–4400. [PubMed: 12805278]
10. Izumikawa M, et al. Auditory hair cell replacement and hearing improvement by Atoh1 gene therapy in deaf mammals. Nat Med 2005;11:271–276. [PubMed: 15711559]
11. Staecker H, Praetorius M, Baker K, Brough DE. Vestibular hair cell regeneration and restoration of balance function induced by math1 gene transfer. Otol Neurotol 2007;28:223–231. [PubMed: 17255891]
12. Knirsch M, et al. Persistence of Ca(v)1.3 Ca_2^+ channels in mature outer hair cells supports outer hair cell afferent signaling. J Neurosci 2007;27:6442–6451. [PubMed: 17567805]
13. Wan L, Almers W, Chen W. Two ribeye genes in teleosts: the role of Ribeye in ribbon formation and bipolar cell development. J Neurosci 2005;25:941–949. [PubMed: 15673675]
14. Brown SD, Hardisty-Hughes RE, Mburu P. Quiet as a mouse: dissecting the molecular and genetic basis of hearing. Nat Rev Genet 2008;9:277–290. [PubMed: 18283275]
15. Friedman LM, Dror AA, Avraham KB. Mouse models to study inner ear development and hereditary hearing loss. Int J Dev Biol 2007;51:609–631. [PubMed: 17891721]
16. Gubbels, S.; Woessner, D.; Mitchell, J.; Brigande, J. *In vivo* electroporation of mouse atonal homolog 1 generates supernumerary and ectopic hair cells in the developing mouse inner ear. Thirtieth Annual MidWinter Research Meeting of the Association for Research in Otolaryngology; 2007. p. 330
17. Kim DW, et al. Use of the human elongation factor 1 alpha promoter as a versatile and efficient expression system. Gene 1990;91:217–223. [PubMed: 2210382]
18. Li X, et al. Generation of destabilized green fluorescent protein as a transcription reporter. J Biol Chem 1998;273:34970–34975. [PubMed: 9857028]
19. Rechsteiner M. PEST sequences are signals for rapid intracellular proteolysis. Semin Cell Biol 1990;1:433–440. [PubMed: 2103894]
20. Sher AE. The embryonic and postnatal development of the inner ear of the mouse. Acta Otolaryngol Suppl 1971;285:1–77. [PubMed: 4334052]
21. Hasson T, et al. Unconventional myosins in inner ear sensory epithelia. J Cell Biol 1997;137:1287–1307. [PubMed: 9182663]
22. Hasson T, et al. Expression in cochlea and retina of myosin VIIa, the gene product defective in Usher syndrome type 1B. Proc Natl Acad Sci U S A 1995;92:9815–9819. [PubMed: 7568224]
23. Chen P, Segil N. p27(Kip1) links cell proliferation to morphogenesis in the developing organ of Corti. Development 1999;126:1581–1590. [PubMed: 10079221]
24. Maklad A, Fritzsch B. Partial segregation of posterior crista and saccular fibers to the nodulus and uvula of the cerebellum in mice, and its development. Brain Res Dev Brain Res 2003;140:223–236.
25. Fritzsch B, et al. Diffusion and imaging properties of three new lipophilic tracers, NeuroVue Maroon, NeuroVue Red and NeuroVue Green and their use for double and triple labeling of neuronal profile. Brain Res Bull 2005;66:249–258. [PubMed: 16023922]
26. Waguespack J, Salles FT, Kachar B, Ricci AJ. Stepwise morphological and functional maturation of mechanotransduction in rat outer hair cells. J Neurosci 2007;27:13890–13902. [PubMed: 18077701]
27. Wu YC, Ricci AJ, Fettiplace R. Two components of transducer adaptation in auditory hair cells. J Neurophysiol 1999;82:2171–2181. [PubMed: 10561397]
28. Li H, Corrales CE, Edge A, Heller S. Stem cells as therapy for hearing loss. Trends Mol Med 2004;10:309–315. [PubMed: 15242678]
29. Hu Z, Ulfendahl M. Cell replacement therapy in the inner ear. Stem Cells Dev 2006;15:449–459. [PubMed: 16846380]
30. Self T, et al. Shaker-1 mutations reveal roles for myosin VIIA in both development and function of cochlear hair cells. Development 1998;125:557–566. [PubMed: 9435277]

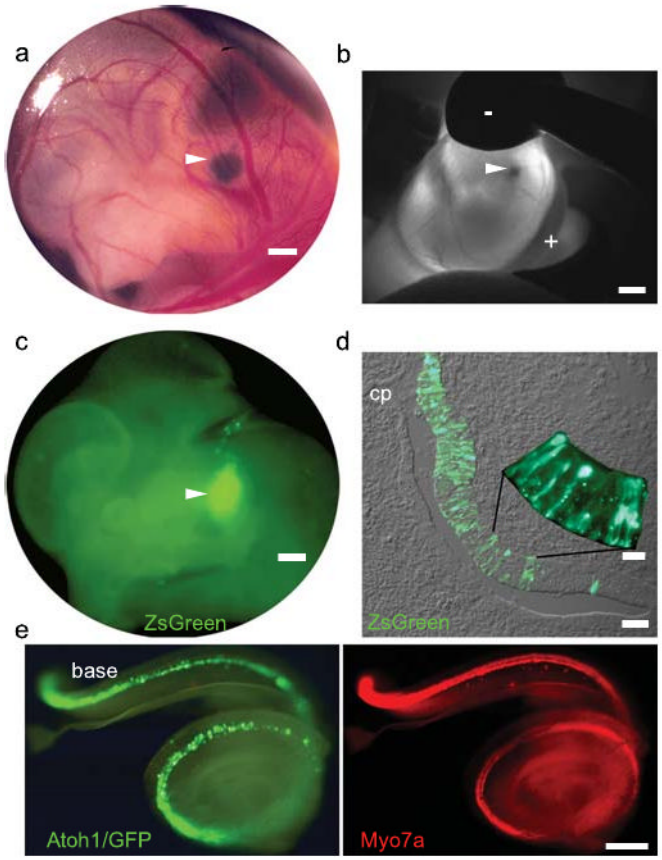

Figure 1. ***In utero*** **gene transfer to the developing mouse inner ear**

a, Expression plasmid was microinjected into the E11.5 otic vesicle. b, The vesicle was centered between the cathode (-) and anode (+) and electroporated. c, Destabilized GFP (ZsGreen) was expressed in the otic territory 24hrs post-electroporation. d, E12.5 progenitors in the medial and ventral otic epithelium expressed ZsGreen robustly. e, E18.5 Atoh1/GFP-transfected cochlea (left) immunostained for Myo7a (right). Arrowheads indicate left otocyst. Scale bars: a, 200μm; b,c, 500μm; d, 50μm; d, inset, 10μm; e, 100μm.

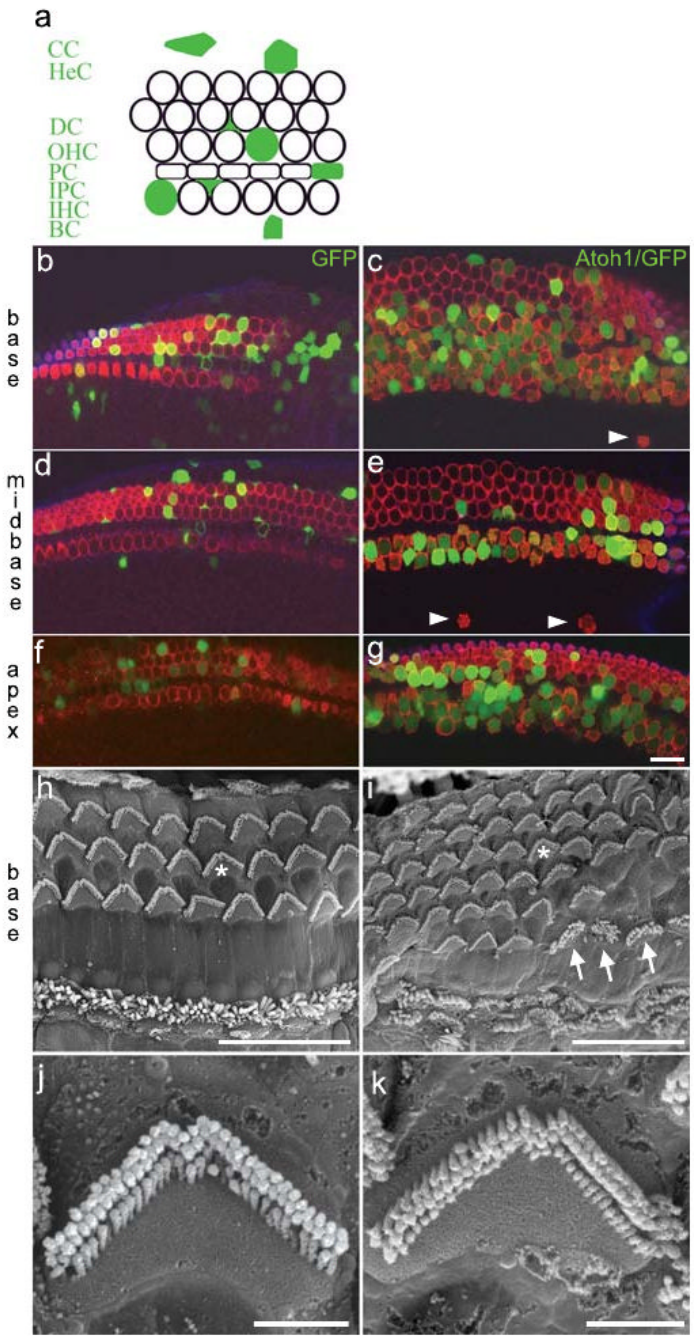

Figure 2. *Atoh1* misexpression generates supernumerary Myo7a$^+$ cells bearing stereociliary bundles

a, schematic of cell types in the organ of Corti transfected with Atoh1/enhanced GFP (filled green): CC, Claudius' cells; HeC, Hensens' cells; DC, Deiters' cells; OHC, outer hair cell; PC, pillar cell; IPC, inner phalangial cell; IHC, inner hair cell; BC, border cell. b-g, laser confocal micrographs of E18.5 GFP-transfected (b,d,f) and Atoh1/GFP-transfected (c,e,g) organs of Corti immunostained for Myo7a (red). All of the Atoh1/GFP$^+$ cells in panels c,e, and g are Myo7a$^+$. h,i, scanning electron micrographs of postnatal day 35, untransfected (h) and Atoh1/GFP-transfected (i) organs of Corti. Asterisks in panels h,i indicate stereociliary

bundles imaged at higher magnification in panels j,k, respectively. The arrows indicate 3 cells with atypical bundles. Scale bars: b-i, 20μm; j,k, 2 μm.

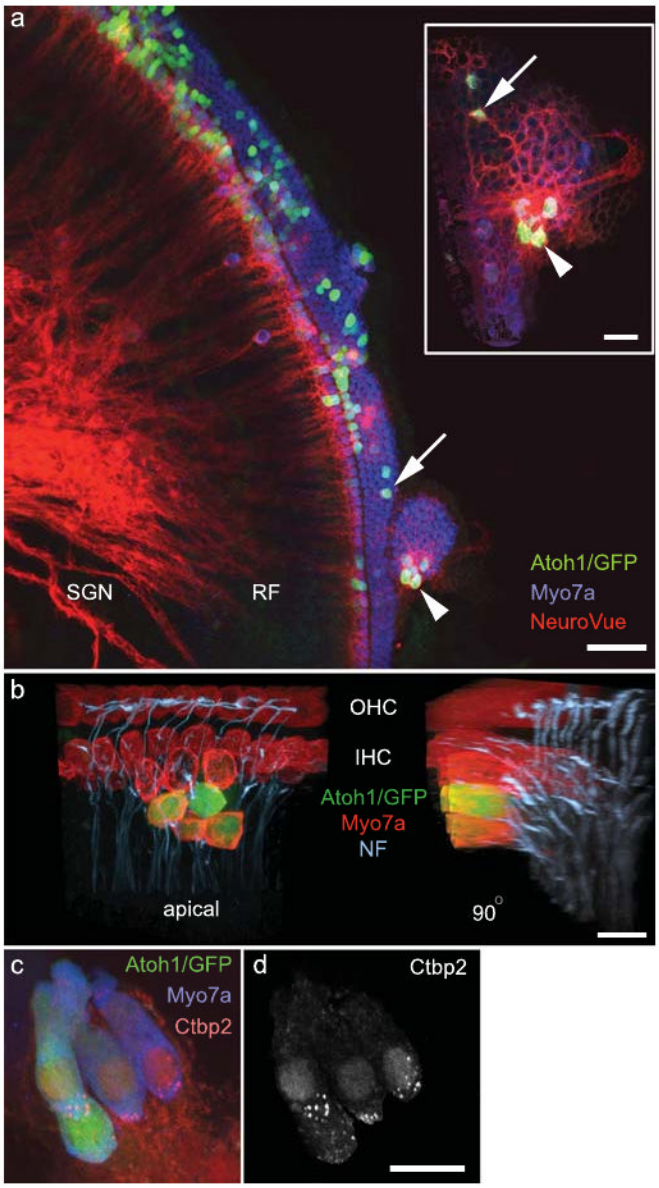

Figure 3. Atoh1/GFP$^+$ cells demonstrate morphological and molecular correlates of innervation and synaptogenesis

a, NeuroVue-Red placed in the cochlear nucleus labels radial fibers (RF) of spiral ganglion neurons (SGN) that project to Atoh1/GFP$^+$/Myo7a$^+$ cells (arrow and arrowhead). Inset shows basal regions of indicated cells. b, Neurofilament$^+$ (NF$^+$) processes associate with Myo7a$^+$ inner and outer hair cells (apical). NF$^+$ processes terminated at the base of an Atoh1/GFP$^+$/Myo7a$^+$ cell cluster as seen in the 90° rotation of the apical 3-dimensional reconstruction. c, Ctbp2 (red) was localized to the basolateral domain at P35. d, The Ctbp2 (red) signal in panel c that was contained within the Myo7a$^+$ hair cell cytoplasm. Scale bars: a, 50 μm; a, inset, 20μm; b-d, 10μm.

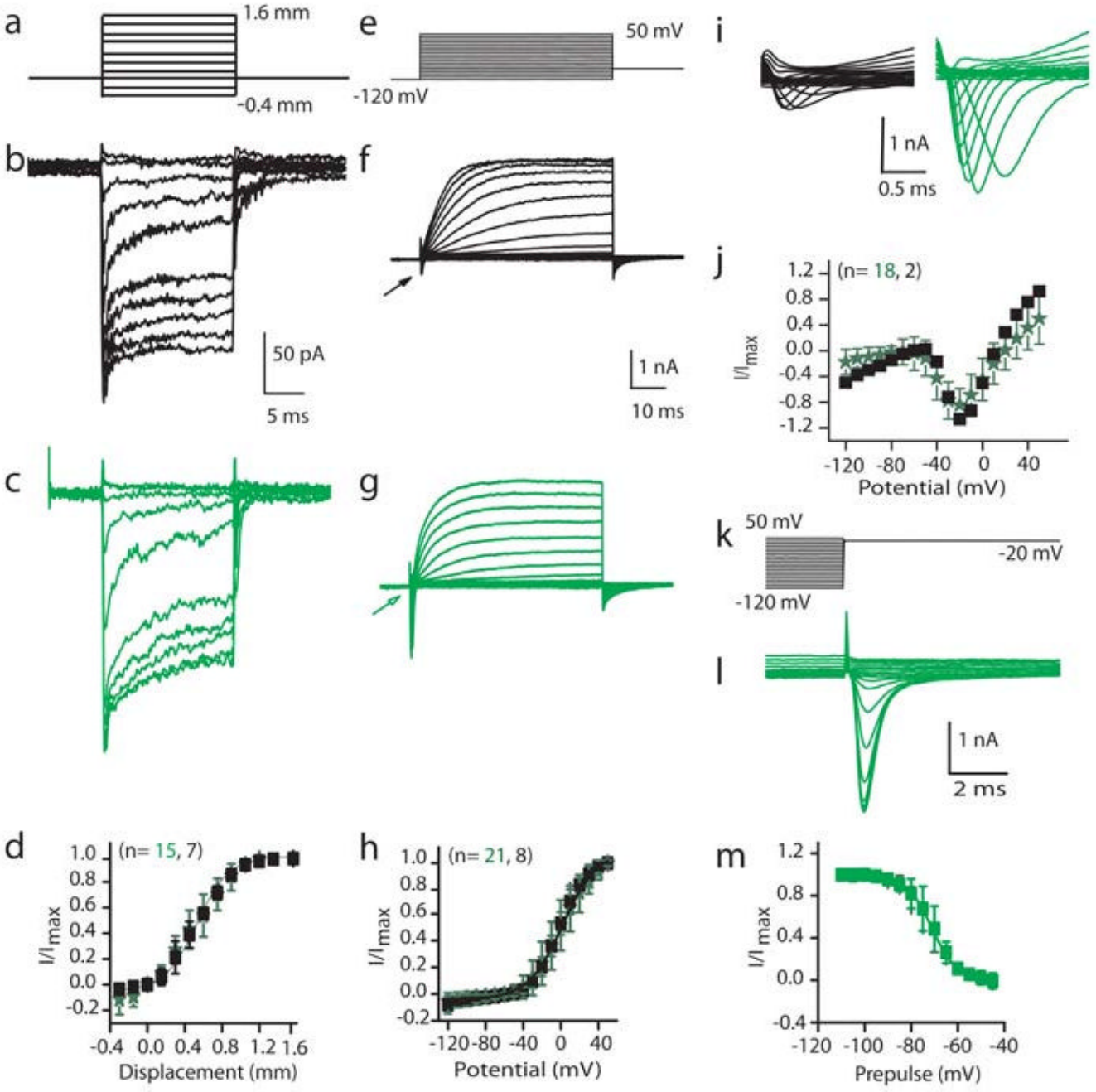

Figure 4. Atoh1/GFP$^+$ cells mechanotransduce and elaborate age-appropriate basolateral conductances

Biophysical response properties of control (black) and GFP$^+$ (green) hair cells. Data are presented as mean ± standard deviation, and two-tailed t-tests were used for statistical comparisons. b, c, Mechanically-evoked currents from a holding potential of -84 mV elicited from the stimulus in a. d, Normalized peak current against displacement; solid line is Boltzmann fit. f, g, Current responses to the voltage-clamp stimuli in e. h, Steady-state current-voltage plot from the data in f,g; solid line is Boltzmann fit. i, The expanded current traces from the regions indicated by arrows in f,g. j, Normalized peak current against potential for inward current. k, Stimulus protocol to probe inactivation that elicited currents

in l. m, Prepulse potential against normalized peak inward current; solid line is Boltzmann fit.